Quantum Spin Ices and Topological Phases from Dipolar-Octupolar Doublets on the Pyrochlore Lattice

Yi-Ping Huang, Gang Chen,* and Michael Hermele
Department of Physics, 390 UCB, University of Colorado, Boulder, Colorado 80309, USA
(Received 13 November 2013; published 25 April 2014)

We consider a class of d- and f-electron systems in which dipolar-octupolar Kramers doublets arise on the sites of the pyrochlore lattice. For such doublets, two components of the pseudospin transform like a magnetic dipole, while the other transforms like a component of the magnetic octupole tensor. Based on a symmetry analysis, we construct and study models of dipolar-octupolar doublets in itinerant and localized limits. In both limits, the resulting models are of surprisingly simple form. In the itinerant limit, we find topological insulating behavior. In the localized limit, the most general nearest-neighbor spin model is the XYZ model. We show that this XYZ model exhibits two distinct quantum spin ice (QSI) phases, that we dub dipolar QSI, and octupolar QSI. We conclude with a discussion of potential relevance to real material systems.

DOI: 10.1103/PhysRevLett.112.167203 PACS numbers: 75.10.Kt, 21.60.Fw, 75.10.Jm, 75.25.Dk

Finding new phases of matter is a problem of fundamental importance in condensed matter physics. This search motivates in part the exploration of new classes of materials, where novel parameter regimes can lead to phases not realized elsewhere, and other new phenomena. Recently, there has been intense interest in materials combining strong spin-orbit coupling (SOC) with substantial electron correlation, especially in compounds with heavy elements [1]. SOC entangles the spin and orbital degrees of freedom, and microscopic models including SOC have, in many cases, not yet been constructed and studied. Spin-orbital entanglement can lead to rather complicated models, but this need not always be the case.

In this Letter, we study a class of systems where strong SOC leads to surprisingly simple microscopic models that—in different limits—naturally realize not only a topological band insulator, but also two distinct quantum spin ice (QSI) phases. One of these is the familiar QSI phase [2,3], here dubbed dipolar QSI (dQSI), while the other is a novel octupolar QSI (oQSI). dQSI and oQSI are two distinct symmetry enriched $\mathrm{U}(1)$ quantum spin liquids, with space group symmetry playing the crucial role.

Much of the recent activity in strong-SOC systems has focused on $5d$ iridates and $4f$ pyrochlores. Various novel models and phases have been predicted for iridates with pyrochlore [4–9], hyperkagome [10–15], honeycomb [16], and hyperhoneycomb lattices [17,18], while the dQSI phase has been predicted in $4f$ pyrochlores [19–23]. In many of these systems, SOC and other interactions lead to Kramers doublets on the d or f ions, which in turn are the building blocks for minimal effective models to capture the low-energy physics. Any Kramers doublet is associated with a time-reversal odd pseudospin operator τ^μ ($\mu = x, y, z$), but not all Kramers doublets transform identically under space group symmetry [24]. The most familiar possibility, which holds in the above recently studied $4f$ and $5d$ systems, is that, just like a true spin-$1/2$ moment, τ^μ transforms as a magnetic dipole (i.e., as a pseudovector) under space group operations.

In this Letter, focusing on the pyrochlore lattice of corner-sharing tetrahedra, we consider a class of systems with Kramers doublets arising from d or f ions, where (in suitable local coordinates discussed below) τ^z and τ^x both transform like the z component of a magnetic dipole, while τ^y transforms as a component of the magnetic octupole tensor. Models of such dipolar-octupolar (DO) doublets have striking properties in both weak and strong correlation limits. We note that a similar type of Kramers doublet has been considered on other lattices [25,26].

More specifically, we consider both $A_2B_2O_7$ pyrochlores and AB_2O_4 spinels, where the pyrochlore A site, and B sites in both families, form a pyrochlore lattice. We consider two principal situations: (1) In both pyrochlores and spinels, B is a transition metal in d^1 or d^3 electron configuration and A is nonmagnetic; (2) in pyrochlores, A is a trivalent rare earth with a partially filled $4f$ shell, and B is nonmagnetic. Both cases can lead to effective models of DO doublets on the pyrochlore lattice.

Case (1).—The magnetic ions reside at the center of a trigonally distorted oxygen octahedron; the single-ion physics has been treated, e.g., in [24]. Because of the cubic crystal field only the t_{2g} manifold is relevant. Projection $\mathcal{P}$ of orbital angular momentum $\mathbf{L}$ into the t_{2g} manifold is $\mathcal{P}\mathbf{L}\mathcal{P} = -\ell$, where the ℓ^μ are spin-1 matrices. The single-site Hamiltonian within the t_{2g} manifold is

$$H = -\lambda \ell \cdot \boldsymbol{S} + H_{\mathrm{tri}} + H_{\mathrm{int}}, \tag{1}$$

with λ the strength of SOC and $\boldsymbol{S}$ the spin operator. $H_{\mathrm{tri}} = \Delta_3 (\ell^{z_i})^2$ is the trigonal crystal field allowed by D_{3d} site

symmetry. The z_i axis is the local C_3 axis ($i = 1, \ldots, 4$ is the sublattice index), and x_i, y_i axes are specified in the Supplemental Material [27]. The interaction $H_{\rm int}$ is of Kanamori form, and is treated in the atomic limit where it is characterized by Hubbard interaction U and Hund's coupling J_H [27].

Defining an effective total angular momentum $\boldsymbol{j}_{\rm eff} = \boldsymbol{\ell} + \boldsymbol{S}$, SOC alone splits the t_{2g} manifold into an upper doublet ($j_{\rm eff} = 1/2$) and lower quadruplet ($j_{\rm eff} = 3/2$). Effective models of $j_{\rm eff} = 1/2$ doublets are relevant for $5d^5$ iridates [28,29] and have received significant attention [4,8,10,16–18]. While the $j_{\rm eff} = 1/2$ doublet is dipolar, it does not obey a naive Heisenberg exchange model due to strong SOC [26,30].

The trigonal crystal field $H_{\rm tri}$ splits the quadruplet into two Kramers doublets, for a total of three doublets. If $\Delta_3 > 0$, the lower and upper doublets are dipolar and transform as the Γ_4^+ irreducible representation of the D_{3d} double group [31]. The middle doublet is a DO doublet; it has $j_{\rm eff}^{z_i} = \pm 3/2$, and transforms as $\Gamma_5^+ \oplus \Gamma_6^+$ (Fig. 1). The doublet is half filled for d^3 electron configuration, or (if $\Delta_3 < 0$) for d^1 configuration.

While Hubbard interaction does not affect the single-site energy spectrum for a fixed number of electrons, Hund's coupling plays an important role. When $\Delta_3 > 0$, we find the d^3 ground state multiplet remains a DO doublet even for large J_H [27]. However, as J_H increases, the energy gap between the ground state and the dipolar doublet first excited state decreases, vanishing in the limit of large J_H where we recover a spin-3/2 moment. The splitting between the ground and first excited doublets is substantial only when $J_H \lesssim \lambda$, and increases with Δ_3/λ [27]. Hund's coupling has no effect for d^1 configuration.

Case (2).—Here A is a trivalent rare earth, where the ground state has angular momentum J. The D_{3d}-symmetric crystal field Hamiltonian is $H_{\rm cf} = 3B_2^0 (J^z)^2 + \cdots$ [32]. If $J = 9/2$ or $15/2$, and $B_2^0 < 0$ and dominates the other crystal field terms, then the ground state is a DO doublet with $J^z = \pm J$, transforming as $\Gamma_5^+ \oplus \Gamma_6^+$ under D_{3d} site

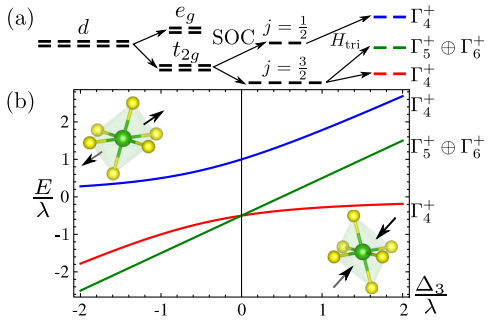

FIG. 1 (color online). (a) The evolution of d electron states under cubic crystal field, SOC, and trigonal distortion. (b) The energies for the three local doublets under different trigonal distortions. Compression (elongation) along the C_3 axis corresponds to $\Delta_3 > 0$ ($\Delta_3 < 0$).

symmetry. The DO doublet nature of the ground state is robust even when the other crystal field terms are appreciable, as long as the ground state is adiabatically connected to the $J^z = \pm J$ doublet. Among the lanthanides, only Nd^{3+}, Dy^{3+}, and Er^{3+} have the required values of J. Of these, $B_2^0 < 0$ only for Nd^{3+} and Dy^{3+} [32]. Indeed, the crystal field ground state of Nd^{3+} in $Nd_2Ir_2O_7$ is a DO doublet [33], and a DO doublet ground state is predicted for Dy^{3+} in $Dy_2Ti_2O_7$[34].

The action of $Fd\bar{3}m$ space group symmetry on DO doublets is given in the Supplemental Material [27]. The D_{3d} site symmetry is generated by a threefold rotation C_3, a mirror plane M, and inversion $\mathcal{I}$, with: $C_3 : \tau^\mu \to \tau^\mu$, $M : \tau^{x,z} \to -\tau^{x,z}$, $M : \tau^y \to \tau^y$, and $\mathcal{I} : \tau^\mu \to \tau^\mu$. These transformations are not those of a pseudovector, and imply that $\tau^{x,z}$ transform like the z_i component of a magnetic dipole, while τ^y transforms like a component of the magnetic octupole tensor [27].

We now proceed to construct effective models using a single DO doublet on each pyrochlore lattice site as the basic building block. We assume throughout that higher-energy on-site degrees of freedom can be ignored. Even when this is not quantitatively accurate, our models may still be valid as minimal low-energy effective models.

We consider limits of itinerant and localized electrons, constructing tight-binding (TB) and spin Hamiltonians, respectively, in the two limits. The Hamiltonian contains all electron hopping terms (itinerant limit) or spin exchange terms (localized limit) allowed by time reversal and $Fd\bar{3}m$ space group symmetry, up to a given spatial range. We note that tight-binding and exchange models of dipolar Γ_4^+ doublets have been extensively studied in the context of iridate and rare-earth pyrochlores [4,9,21,22,35–37].

In the itinerant limit, we ignore electron interactions, and the general form of the model is

$$H_{TB} = \sum_{(\boldsymbol{r},\boldsymbol{r}')} [c_{\boldsymbol{r}}^\dagger T_{\boldsymbol{r}\boldsymbol{r}'} c_{\boldsymbol{r}} + \text{H.c.}]. \tag{2}$$

Here, $\boldsymbol{r}$ labels pyrochlore lattice sites, the sum is over all pairs of sites, and $c_{\boldsymbol{r}}^T = (c_{\boldsymbol{r}+}, c_{\boldsymbol{r}-})$. $T_{\boldsymbol{r}\boldsymbol{r}'} = T_{\boldsymbol{r}'\boldsymbol{r}}^\dagger$ is a 2×2 matrix describing tunneling between sites $\boldsymbol{r}$ and $\boldsymbol{r}'$. The operator $c_{\boldsymbol{r}\pm}^\dagger$ creates an electron at site $\boldsymbol{r}$ with $j_{\rm eff}^{z_i} = \pm 3/2$ in case (1), or $J^{z_i} = \pm J$ in case (2). Pseudospin operators are $\tau_{\boldsymbol{r}}^\mu = (1/2) c_{\boldsymbol{r}}^\dagger \sigma^\mu c_{\boldsymbol{r}}$, where σ^μ are the Pauli matrices. Time reversal symmetry implies $T_{\boldsymbol{r}\boldsymbol{r}'} = t_{\boldsymbol{r}\boldsymbol{r}'}^0 + i t_{\boldsymbol{r}\boldsymbol{r}'}^\mu \sigma^\mu$.

For nearest-neighbor sites, the hopping matrix $T_{\boldsymbol{r}\boldsymbol{r}'}$ has a remarkably simple form. Choosing an appropriate orientation of bonds [27], we find $T_{\boldsymbol{r}\boldsymbol{r}'} = i[t_{nn}^1 \sigma^1 + t_{nn}^3 \sigma^3]$, taking the same form for all nearest-neighbor bonds. A global rotation about the y axis in pseudospin space can, thus, eliminate t_{nn}^1, leading to $\tilde{T}_{\boldsymbol{r}\boldsymbol{r}'} = i\tilde{t}_{nn}^3 \sigma^3$, where the tilde indicates we are working in the transformed basis. Thus, the nearest-neighbor model has a U(1) spin symmetry, and the purely imaginary (spin-dependent) hopping is similar

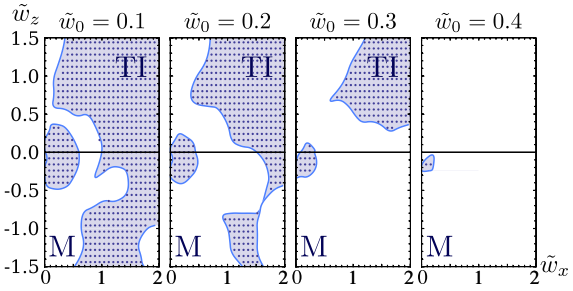

FIG. 2 (color online). Phase diagram of the tight-binding model wtih first- and second-neighbor hopping, as a function of $(\tilde{w}_0, \tilde{w}_x, \tilde{w}_z)$, setting $\tilde{t}^3_{nn} = 1$. Very small fourth-neighbor hopping is included to remove unstable band touchings at the W point. Metallic (M) and strong topological insulator (TI) phases are found. The phase diagram is symmetric under $\tilde{w}_x \to -\tilde{w}_x$ and $\tilde{w}_0 \to -\tilde{w}_0$.

to models considered in [38]. A highly unstable Fermi surface coincides with a surface of intersection between two bands [27].

Evidently the nearest-neighbor tight-binding model is highly fine tuned, so we also include second-neighbor hopping, which is specified by parameters $(\tilde{w}_0, \tilde{w}_x, \tilde{w}_z)$ [27]. Second-neighbor hopping breaks the U(1) spin symmetry and gaps out most of the nearest-neighbor Fermi surface. One finds either a metallic state, or a semimetal with isolated band touchings occurring at the W points (see Fig. 2). These W-point touchings are, in fact, unstable and are gapped out by fourth-neighbor hopping, leading to a strong topological band insulator [27].

We now consider the large-U limit of localized electrons, where the degrees of freedom are the pseudospin$-1/2$ moments $\tau^{\mu}_{\mathbf{r}}$. We find that the most general symmetry allowed nearest-neighbor exchange is $H_{ex} = \sum_{\langle \mathbf{r}\mathbf{r}'\rangle}[J_x \tau^x_{\mathbf{r}} \tau^x_{\mathbf{r}'} + J_y \tau^y_{\mathbf{r}} \tau^y_{\mathbf{r}'} + J_z \tau^z_{\mathbf{r}} \tau^z_{\mathbf{r}'} + J_{xz}(\tau^x_{\mathbf{r}} \tau^z_{\mathbf{r}'} + \tau^z_{\mathbf{r}} \tau^x_{\mathbf{r}'})]$, where the sum is over nearest-neighbor bonds. Quite remarkably, the exchange is identical in form on every bond. Similar to the itinerant limit, the J_{xz} term can be eliminated by a global pseudospin rotation [27]. After this transformation, the exchange is of the remarkably simple XYZ form

$$H_{XYZ} = \sum_{\langle \mathbf{r}\mathbf{r}'\rangle} \tilde{J}_x \tilde{\tau}^x_{\mathbf{r}} \tilde{\tau}^x_{\mathbf{r}'} + \tilde{J}_y \tilde{\tau}^y_{\mathbf{r}} \tilde{\tau}^y_{\mathbf{r}'} + \tilde{J}_z \tilde{\tau}^z_{\mathbf{r}} \tilde{\tau}^z_{\mathbf{r}'}. \tag{3}$$

This result should be contrasted with the case of dipolar doublets on the pyrochlore lattice, where the form of nearest-neighbor exchange varies according to the orientation of each bond [20].

Beyond simplicity of form, this pyrochlore XYZ model supports two distinct QSI phases. To see this, we first review the XXZ model ($\tilde{J}_\perp \equiv \tilde{J}_x = \tilde{J}_y$), where QSI was identified in a study of the regime $\tilde{J}_z > 0$, $\tilde{J}_z \gg |\tilde{J}_\perp|$ [2]. For simplicity, we concentrate on $\tilde{J}_\perp < 0$, where quantum Monte Carlo calculations [39] found QSI for $|\tilde{J}_\perp|/\tilde{J}_z < c$, with $c \approx 0.1$. When $|\tilde{J}_\perp|/\tilde{J}_z > c$, magnetic order is present.

It is important to note that QSI is robust to arbitrary symmetry breaking perturbations, and thus, survives away from the XXZ line.

The physics of QSI can be understood by mapping to a compact U(1) gauge theory, which is exact for large $\tilde{J}_z$ [2]. The centers of pyrochlore lattice tetrahedra $\mathbf{r}$ form a diamond lattice, and each pyrochlore site $\boldsymbol{r}$ corresponds to a unique nearest-neighbor diamond link $(\mathbf{r}, \mathbf{r}')$. We introduce lattice vector fields $E_{\mathbf{r}\mathbf{r}'} = \tilde{\tau}^z_{\boldsymbol{r}}$ and $e^{iA_{\mathbf{r}\mathbf{r}'}} = \tilde{\tau}^x_{\boldsymbol{r}} + i\tilde{\tau}^y_{\boldsymbol{r}}$, where $\mathbf{r}$ ($\mathbf{r}'$) lies in the diamond A (B) sublattice, and $E_{\mathbf{r}\mathbf{r}'} = -E_{\mathbf{r}'\mathbf{r}}$, $A_{\mathbf{r}\mathbf{r}'} = -A_{\mathbf{r}'\mathbf{r}}$. E (A) can be interpreted as the electric field (vector potential) of a compact U(1) lattice gauge theory, of which QSI is the deconfined phase, supporting a gapless photon, and gapped electric charge and magnetic monopole excitations.

So far, we have been describing dQSI, so named because the electric field $E_{\mathbf{r}\mathbf{r}'} = \tilde{\tau}^z_{\boldsymbol{r}}$ is a magnetic dipole. In the low-energy continuum theory, the electric field is odd under time reversal and transforms under the Γ^+_4 (pseudovector) representation of the O_h point group. [The magnetic field is time reversal even, and transforms under the Γ^-_4 (vector) representation.] The same dQSI phase occurs for large $\tilde{J}_x > 0$ ($\tilde{J}_{y,z} < 0$ for simplicity), where $E_{\mathbf{r}\mathbf{r}'} = \tilde{\tau}^x_{\boldsymbol{r}}$, which transforms identically to $\tilde{\tau}^z_{\boldsymbol{r}}$ under symmetry.

The novel oQSI phase arises for $\tilde{J}_y > 0$ large ($\tilde{J}_{x,z} < 0$ for simplicity), so that $E_{\mathbf{r}\mathbf{r}'} = \tilde{\tau}^y_{\boldsymbol{r}}$. In this case, the electric field is purely octupolar. In the continuum theory, the electric field is still time reversal odd, but transforms under the Γ^+_5 representation of O_h (neither vector nor pseudovector). The magnetic field transforms as Γ^-_5.

Thus, oQSI and dQSI are distinguished by the action of space group symmetry on electric and magnetic fields, and can be viewed as distinct symmetry enriched U(1) quantum spin liquids. This means that dQSI and oQSI are distinct phases in the presence of space group symmetry, but weak space-group-breaking perturbations take dQSI and oQSI into the same U(1) quantum spin liquid phase (which is robust to arbitrary weak perturbations regardless of symmetry). In terms of physical properties, dQSI and oQSI both have a T^3 contribution to specific heat from gapless photons; in f-electron realizations, this is expected to be about 1000 times the phonon contribution [21]. Dipolar spin correlations, as measured, e.g., by neutron scattering, will, however, be quite different, as illustrated by the fact that, neglecting effects of long-range dipolar interaction, equal-time dipolar correlations fall off as $1/r^4$ in dQSI [2], but as $1/r^8$ in oQSI [27]. In future work, it would be interesting to compare the dynamic spin structure factor in dQSI and oQSI. Neutron scattering signatures of dQSI have been discussed in [21].

So far, we have avoided discussing the case $\tilde{J}_\perp > 0$; here, less is known for the XXZ model, due to the presence of a sign problem in quantum Monte Carlo calculations. In the $|\tilde{J}_\perp|/\tilde{J}_z \ll 1$ limit, $\tilde{J}_\perp$ favors QSI with π flux of the vector potential $A_{\mathbf{r}\mathbf{r}'}$ through each pyrochlore hexagon,

unlike for $\tilde{J}_\perp < 0$, where zero flux is favored [27]. We have not considered the properties of the resulting π-flux versions of dQSI and oQSI, leaving this for future work. QSI is expected to persist over a larger range of $\tilde{J}_\perp > 0$, since, in this case, both $\tilde{J}_z$ and $\tilde{J}_\perp$ interactions are frustrated [22].

We now discuss the phase diagram of the XYZ model. The simplest magnetically ordered phases appear ferromagnetic in local coordinates; for instance, if $\tilde{J}_z < 0$ and is dominant, $\langle \tilde{\tau}^z_{\mathbf{r}} \rangle = m_d \neq 0$. This is the "all-in-all-out" (AIAO) state, where dipoles point along the local z_i axes, toward (away from) pyrochlore tetrahedron centers lying in the diamond A (B) sublattices (or vice versa). Since τ^z and τ^x transform identically under space group, the same AIAO state arises when $\tilde{J}_x < 0$, $|\tilde{J}_x| \gg \tilde{J}_{y,z}$. A distinct magnetically ordered phase, with $\langle \tilde{\tau}^y_{\mathbf{r}} \rangle = m_o \neq 0$, is obtained when $\tilde{J}_y < 0$, $|\tilde{J}_y| \gg \tilde{J}_{x,z}$. This state has antiferro-octupolar (AFO) order, and no on-site dipolar order.

To study the phase diagram away from the simple limits discussed above, we employ gauge mean field theory (gMFT) [21,22] to our model [27]. gMFT makes the U(1) gauge structure explicit via a slave particle construction, and is capable of describing both QSI and magnetic phases. For simplicity, we limited our analysis to the shaded regions shown (Fig. 3) on the faces of a cube in $(\tilde{J}_x, \tilde{J}_y, \tilde{J}_z)$ space. We find only the two QSI and magnetically ordered phases discussed above. In the same regions of parameter space we analyzed via gMFT, the XYZ model can be studied via quantum Monte Carlo calculations without a sign problem [27].

We now comment on the prospects for applying the models discussed above to real materials. Promising systems to realize the XYZ model are $Nd_2B_2O_7$ pyrochlores. B = Zr, Sn compounds are insulators exhibiting antiferromagnetic order at low temperature [40,41]. While the B = Ir compound is known to carry a DO doublet [33], the physics is complicated by the presence of Ir conduction electrons [7]. Synthesis of other Nd pyrochlores has been reported [42]. The validity of the XYZ model description could be ascertained and the exchange couplings measured directly via neutron scattering in applied magnetic field, as was done in the dipolar case for $Yb_2Ti_2O_7$ [43]. DO doublets are likely in Dy pyrochlores [34], but the large moment of Dy^{3+} means dipolar interactions must be included. DO doublets may also occur in B-site rare earth spinels, and there is evidence for this in $CdEr_2Se_4$ [44]. More broadly, strongly localized d-electron Mott insulators with $S = 3/2$ and D_{3d} site symmetry comprise another class of systems where DO doublets may be the low-energy degrees of freedom.

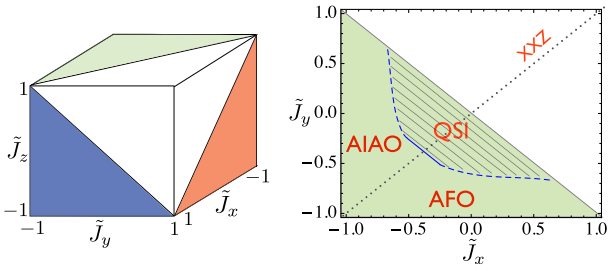

FIG. 3 (color online). Left: Unit cube in $(\tilde{J}_x, \tilde{J}_y, \tilde{J}_z)$ parameter space of the XYZ model. Shaded regions were analyzed via gMFT. Right: gMFT phase diagram on the $\tilde{J}_z = 1$ surface of the cube, where dQSI, AIAO, and AFO phases are found. Within gMFT, the phase transition is 1st order (2nd order) at the dashed (solid) boundary. The dotted line is the XXZ line. We did not apply gMFT for $\tilde{J}_x + \tilde{J}_y \geq 0$. There, the exchange is frustrated, and QSI is likely to be more stable than for $\tilde{J}_x + \tilde{J}_y < 0$ [22]. The phase diagram on the other surfaces of the cube can be obtained by relabeling parameters, with the nature of phases changing according to the anisotropic character of $\tilde{\tau}^\mu_{\mathbf{r}}$. dQSI occurs on the $\tilde{J}_z = 1$ and $\tilde{J}_x = 1$ faces, while oQSI occurs on the $\tilde{J}_y = 1$ face.

5d systems are a likely setting for itinerant (or weakly localized) DO doublets. $Cd_2Os_2O_7$, believed to exhibit AIAO order below a finite-temperature metal-insulator transition [45,46], has Os^{3+} in $5d^3$ configuration. Microscopic calculations indicate a DO doublet ground state, but show a very small splitting between ground and first excited doublets [47], likely due to Hund's coupling. Moreover, electronic structure calculations do not show a clear separation between DO doublet and other energy bands [48,49]. Thus, $5d^1$ systems, perhaps on other lattices, may be more promising for the realization of itinerant DO doublets.

In summary, we have pointed out that Kramers doublets with dipolar-octupolar character can arise on the sites of the pyrochlore lattice in both d- and f-electron systems. We studied effective models of DO doublets in itinerant and localized limits, finding topological insulation in the former case, and two distinct quantum spin ice phases in the latter.

We thank Leon Balents, Michel Gingras, Sungbin Lee, and Lucile Savary for helpful conversations and correspondence. This work was supported by the U.S. Department of Energy, Office of Science, Basic Energy Sciences, under Award No. DE-FG02-10ER46686.

*Present address: Department of Physics, University of Toronto, Toronto, Ontario M5S 1A7, Canada.

[1] W. Witczak-Krempa, G. Chen, Y. B. Kim, and L. Balents, Annu. Rev. Condens. Matter Phys. **5**, 57 (2014).
[2] M. Hermele, M. P. A. Fisher, and L. Balents, Phys. Rev. B **69**, 064404 (2004).
[3] M. J. P. Gingras and P. A. McClarty, arXiv:1311.1817.
[4] D. Pesin and L. Balents, Nat. Phys. **6**, 376 (2010).
[5] X. Wan, A. M. Turner, A. Vishwanath, and S. Y. Savrasov, Phys. Rev. B **83**, 205101 (2011).
[6] M. Kargarian, J. Wen, and G. A. Fiete, Phys. Rev. B **83**, 165112 (2011).
[7] G. Chen and M. Hermele, Phys. Rev. B **86**, 235129 (2012).
[8] W. Witczak-Krempa and Y. B. Kim, Phys. Rev. B **85**, 045124 (2012).

[9] W. Witczak-Krempa, A. Go, and Y. B. Kim, Phys. Rev. B **87**, 155101 (2013).
[10] G. Chen and L. Balents, Phys. Rev. B **78**, 094403 (2008).
[11] Y. Zhou, P. A. Lee, T.-K. Ng, and F.-C. Zhang, Phys. Rev. Lett. **101**, 197201 (2008).
[12] M. J. Lawler, H.-Y. Kee, Y. B. Kim, and A. Vishwanath, Phys. Rev. Lett. **100**, 227201 (2008).
[13] M. J. Lawler, A. Paramekanti, Y. B. Kim, and L. Balents, Phys. Rev. Lett. **101**, 197202 (2008).
[14] E. J. Bergholtz, A. M. Läuchli, and R. Moessner, Phys. Rev. Lett. **105**, 237202 (2010).
[15] G. Chen and Y. B. Kim, Phys. Rev. B **87**, 165120 (2013).
[16] J. Chaloupka, G. Jackeli, and G. Khaliullin, Phys. Rev. Lett. **105**, 027204 (2010).
[17] I. Kimchi, J. G. Analytis, and A. Vishwanath, arXiv:1309.1171.
[18] E. K.-H. Lee, R. Schaffer, S. Bhattacharjee, and Y. B. Kim, Phys. Rev. B **89**, 045117 (2014).
[19] H. R. Molavian, M. J. P. Gingras, and B. Canals, Phys. Rev. Lett. **98**, 157204 (2007).
[20] S. Onoda and Y. Tanaka, Phys. Rev. B **83**, 094411 (2011).
[21] L. Savary and L. Balents, Phys. Rev. Lett. **108**, 037202 (2012).
[22] S. B. Lee, S. Onoda, and L. Balents, Phys. Rev. B **86**, 104412 (2012).
[23] R. Applegate, N. R. Hayre, R. R. P. Singh, T. Lin, A. G. R. Day, and M. J. P. Gingras, Phys. Rev. Lett. **109**, 097205 (2012).
[24] A. Abragam and B. Bleaney, *Electron Paramagnetic Resonance of Transition Ions*, Oxford Classic Texts in the Physical Sciences (Oxford University Press, New York, 1970).
[25] G. Jackeli and G. Khaliullin, Phys. Rev. Lett. **103**, 067205 (2009).
[26] G. Chen, R. Pereira, and L. Balents, Phys. Rev. B **82**, 174440 (2010).
[27] See Supplemental Material at http://link.aps.org/supplemental/10.1103/PhysRevLett.112.167203 for discussion of Hund's coupling, detailed symmetry analyses, details of gauge mean-field theory, and other technical details.
[28] B. J. Kim, H. Jin, S. J. Moon, J.-Y. Kim, B.-G. Park, C. S. Leem, J. Yu, T. W. Noh, C. Kim, S.-J. Oh, *et al.*, Phys. Rev. Lett. **101**, 076402 (2008).
[29] B. J. Kim, H. Ohsumi, T. Komesu, S. Sakai, T. Morita, H. Takagi, and T. Arima, Science **323**, 1329 (2009).
[30] G. Chen and L. Balents, Phys. Rev. B **84**, 094420 (2011).
[31] G. F. Koster, J. O. Dimmock, R. G. Wheeler, and H. Statz, *The Properties of the Thirty-Two Point Groups*, MIT Research Monographs, No. 34 (MIT, Cambridge, MA, 1963).
[32] J. S. Gardner, M. J. P. Gingras, and J. E. Greedan, Rev. Mod. Phys. **82**, 53 (2010).
[33] M. Watahiki, K. Tomiyasu, K. Matsuhira, K. Iwasa, M. Yokoyama, S. Takagi, M. Wakeshima, and Y. Hinatsu, J. Phys. Conf. Ser. **320**, 012080 (2011).
[34] A. Bertin, Y. Chapuis, P. D. de Rotier, and A. Yaouanc, J. Phys. Condens. Matter **24**, 256003 (2012).
[35] S. H. Curnoe, Phys. Rev. B **78**, 094418 (2008).
[36] M. Kurita, Y. Yamaji, and M. Imada, J. Phys. Soc. Jpn. **80**, 044708 (2011).
[37] W. Witczak-Krempa and Y. B. Kim, Phys. Rev. B **85**, 045124 (2012).
[38] F. J. Burnell, S. Chakravarty, and S. L. Sondhi, Phys. Rev. B **79**, 144432 (2009).
[39] A. Banerjee, S. V. Isakov, K. Damle, and Y. B. Kim, Phys. Rev. Lett. **100**, 047208 (2008).
[40] H. W. J. Blöte, R. F. Wielinga, and W. J. Huiskamp, Physica (Utrecht) **43**, 549 (1969).
[41] K. Matsuhira, Y. Hinatsu, K. Tenya, H. Amitsuka, and T. Sakakibara, J. Phys. Soc. Jpn. **71**, 1576 (2002).
[42] M. A. Subramanian, G. Aravamudan, and G. V. S. Rao, Prog. Solid State Chem. **15**, 55 (1983).
[43] K. A. Ross, L. Savary, B. D. Gaulin, and L. Balents, Phys. Rev. X **1**, 021002 (2011).
[44] J. Lago, I. Živković, B. Z. Malkin, J. Rodriguez Fernandez, P. Ghigna, P. Dalmas de Réotier, A. Yaouanc, and T. Rojo, Phys. Rev. Lett. **104**, 247203 (2010).
[45] A. Koda, R. Kadono, K. Ohishi, S. R. Saha, W. Higemoto, S. Yonezawa, Y. Muraoka, and Z. Hiroi, J. Phys. Soc. Jpn. **76**, 063703 (2007).
[46] J. Yamaura, K. Ohgushi, H. Ohsumi, T. Hasegawa, I. Yamauchi, K. Sugimoto, S. Takeshita, A. Tokuda, M. Takata, M. Udagawa, *et al.*, Phys. Rev. Lett. **108**, 247205 (2012).
[47] N. A. Bogdanov, R. Maurice, I. Rousochatzakis, J. van den Brink, and L. Hozoi, Phys. Rev. Lett. **110**, 127206 (2013).
[48] D. J. Singh, P. Blaha, K. Schwarz, and J. O. Sofo, Phys. Rev. B **65**, 155109 (2002).
[49] H. Shinaoka, T. Miyake, and S. Ishibashi, Phys. Rev. Lett. **108**, 247204 (2012).